

n-Doping of thermally polymerizable fullerenes as an electron transporting layer for inverted polymer solar cells†

Namchul Cho, Hin-Lap Yip, Steven K. Hau, Kung-Shih Chen, Tae-Wook Kim, Joshua A. Davies, David F. Zeigler and Alex K.-Y. Jen*

Received 14th January 2011, Accepted 11th March 2011

DOI: 10.1039/c1jm10214a

A novel [6,6]-phenyl-C₆₁-butyric acid methyl styryl ester (PCBM-S) was synthesized and employed as an electron transporting interfacial layer for bulk heterojunction polymer solar cells with an inverted device configuration. After the deposition of PCBM-S film from solution, the styryl groups of PCBM-S were polymerized by post-thermal treatment to form a robust film which is resistive to common organic solvents. This allows the solution processing of upper bulk heterojunction film without eroding the PCBM-S layer. Additionally, the PCBM-S was n-doped with decamethylcobaltocene (DMC) to increase the conductivity of the film, which resulted in a significantly improved power conversion efficiency from 1.24% to 2.33%. The improved device performance is due to the decrease of series resistance and improved electron extraction property of the n-doped PCBM-S film.

1. Introduction

Polymer solar cells (PSCs) are a promising source of low-cost alternative energy due to their potential scalability and the ease of fabrication.^{1–3} Recently, a very encouraging device performance of greater than 7% power conversion efficiency (PCE) has been demonstrated.^{4,5} The improvement of PCE was realized by the development of novel donor polymers,^{6–9} fullerene acceptors,^{10,11} and optimization of the bulk heterojunction (BHJ) morphology.^{12–14} Apart from the importance of achieving higher PCEs, improving the stability of PSCs is equally important. In general, PSCs with a conventional structure are comprised of a BHJ active layer sandwiched between an indium tin oxide (ITO) anode and a low work-function metal cathode. However, low work-function metal electrodes are quite unstable under ambient conditions.¹⁵ To overcome this problem, PSCs with an inverted device structure had been developed which enables the use of stable and printable high work-function metals as hole collecting top electrodes and low work-function metal oxide as electron collecting bottom electrodes. This results in significantly improved stability in an ambient environment.^{16,17}

Reversing the polarity of charge-collecting electrodes in inverted PSC can be achieved by adopting appropriate electron-transporting and hole-transporting materials between the ITO/BHJ and BHJ/metal interfaces, respectively. Efficient interfacial materials should possess several desired physical, chemical, and

electronic properties including (1) appropriate energy level matching between the electrodes and the active layer to facilitate unipolar charge extraction to the corresponding electrode; (2) high conductivities to minimize the Ohmic loss from series resistance; (3) high solvent resistance to facilitate multilayer film deposition from solutions; (4) low optical absorption to maximize the number of photons reaching the active layer; and (5) chemically inert to prevent interfacial reactions with electrodes for achieving long-term stability.

Several classes of materials had been explored as possible electron selective materials for inverted PSCs. The most widely studied ones are n-type inorganic metal oxides including titanium oxide¹⁸ and zinc oxide.^{19,20} Despite their good electron selective properties, the sensitivity of their electrical properties to the surface adsorption of oxygen and UV-irradiation may complicate the use of these materials in PSCs.^{21–23} Modifications of the metal oxide surface using fullerene-based self-assembled monolayers^{24,25} or thin films²⁶ had been demonstrated as an efficient strategy to further improve the interfacial properties between metal oxide and BHJ film. These have resulted in enhanced device efficiency and stability. Ultra-thin insulating aluminium oxide²⁷ and cesium oxide obtained through thermal decomposition of cesium salt²⁸ have also been used to modify the ITO work functions to facilitate electron collection in inverted cells.

Although a large number of studies have been performed on n-type inorganic interfacial materials, only few attempts have been made on polymer or small molecule based n-type interfacial materials for inverted PSCs even though they have great advantages compared to inorganic materials, such as the versatility of tuning their optical, electrical, and physical properties through organic synthesis. In addition, polymeric materials are

Department of Materials Science and Engineering, University of Washington, Seattle, Washington, 98195, USA. E-mail: ajen@u.washington.edu; Fax: +1 206 543 3100; Tel: +1 206 543 2626

† Electronic supplementary information (ESI) available. See DOI: 10.1039/c1jm10214a

intrinsically more flexible, making them a better option for plastic solar cells that are bendable and rugged.

One of the limiting factors for directly using conjugated polymers or small molecules as interfacial materials in organic solar cells is their relatively low conductivities, which results in high series resistance and poor Ohmic contact with the electrodes.²⁹ As a result, improving the conductivity of interfacial transport layers through chemical doping is required for the realization of high performance solar cells. This strategy has been widely used in vacuum-evaporated small molecule-based solar cells in which the small molecule semiconductor and dopant can be co-deposited to achieve controllable and stable doping.²⁹ However, chemical doping of solution processed transport layer is more challenging. Unlike small molecule-based multilayer devices that can be fabricated by subsequent deposition through vacuum processes, polymer-based interfacial materials should possess good solvent resistance to prevent solvent-induced erosion during the multi-layer film deposition process. In addition, concurrent development of stable dopants that are compatible with solution processing is necessary.

Thermal- or photo-crosslinkable charge-transporting materials had been demonstrated as efficient interfacial materials that provide adequate solvent resistance for the fabrication of polymer light-emitting diodes.³⁰ This class of materials has also been employed as hole-transporting layers in PSCs to improve the hole collection property.^{31–33} Recently, cross-linkable fullerene materials were developed and employed as n-type interfacial layers between ZnO and the active layer to enhance the electron collection property in inverted PSCs.²⁶ However, without ZnO, fullerene is ineffective as a good electron-transporting material (ETM) in inverted PSCs because of its low conductivity compared to metal oxides. Therefore, n-doping of fullerene is required to enhance the conductivity of the electron-transporting layer. n-Type doping has been studied in vacuum-deposited small molecule based solar cells in which the fullerene electron-transporting layer is doped with decamethylcobaltocene (DMC) to achieve significantly improved PCE compared to the undoped cells.³⁴

A crystallographic study of the fullerene complex with DMC reported by Konarev *et al.* showed that the fullerene anion and DMC cation form a stable three-dimensional framework with solvent molecules.³⁵ Because the solid-state ionization energy of DMC (3.3 eV)³⁴ is smaller than the LUMO of PCBM-S (~3.7 eV), efficient n-doping of PCBM-S can be achieved through electron transfer from the HOMO of the dopant to the LUMO of the fullerene derivative.

The focus of the current study is to demonstrate the improved device performance of inverted PSCs by incorporating robust fullerene side-chain polymers that are chemically doped with DMC to form an efficient electron-transporting interfacial layer. The fullerene polymer films produced by thermal polymerization on ITO substrates possess good solvent resistance. Chemical n-doping of fullerene polymers with DMC is shown to significantly enhance the PCE. The improved device performance is attributed to the decreased series resistance and efficient electron extraction *via* the n-doped PCBM-S polymer films. We also investigate n-channel organic thin-film transistors (OTFTs) using n-doped fullerene polymers to characterize the effect of doping on the electrical properties of the PCBM-S.

2. Experimental section

Materials synthesis

All chemicals were purchased from Aldrich Chemical Corporation unless otherwise specified. Regio-regular poly(3-hexylthiophene) (P3HT) and PCBM were purchased from Rieke Metals, Inc. and American Dye Source, Inc, respectively, and were used as received. 4-Vinylbenzyl alcohol (**2**) and PCBA were synthesized according to literature methods.^{36,37}

Synthesis of PCBM-S

A solution of PCBA (40 mg, 0.045 mmol), 4-vinylbenzyl alcohol (8.97 mg, 0.067 mmol) and 4-dimethylaminopyridine-4-toluenesulfonate (19.67 mg, 0.067 mmol) in dichloromethane (30 mL) in a round bottom flask was stirred for 5 min at room temperature. After 5 min, 1,3-diisopropyl carbodiimide (28.14 mg, 0.225 mmol) was added and the solution was allowed to stir for 12 hours. The coupling reaction was monitored by thin-layer chromatography. After removal of solvent, the crude product was purified by column chromatography using toluene/hexane (1 : 1, v/v). The PCBM-S was collected by filtration and washed with methanol to give a brown solid (20 mg, 55% yield). ¹H NMR (300 MHz, CDCl₃, 25 °C, TMS): δ = 2.19 (m, 2H), 2.59 (t, 2H), 2.93 (m, 2H), 5.12 (s, 2H), 5.32 (d, J = 16.8, 1H), 5.80 (d, J = 18.3, 1H), 6.68 (q, J = 10.8, 1H), 7.28–7.59 (m, 7H), 7.93 (d, J = 4.8, 2H); ¹³C NMR (125 MHz, CDCl₃, 25 °C, TMS): δ = 22.4, 33.7, 34.1, 51.9, 66.2, 79.9, 114.4, 128.3, 128.5, 128.6, 132.1, 135.3, 136.3, 137.6, 138.1, 140.8, 141.0, 142.1, 142.2, 142.2, 142.3, 142.9, 143.0, 143.1, 143.8, 144.0, 144.4, 144.5, 144.7, 144.8, 145.1, 145.1, 145.2, 145.9, 147.8, 148.8. Anal. Calcd for C₈₀H₂₀: C, 94.85, H, 1.99. Found: C, 93.28, H, 1.48%.

Absorption, thermal property and morphology measurements

A Perkin-Elmer Lambda-9 spectrophotometer was used to measure UV-Vis spectra. The thermal property was studied using differential scanning calorimetry (DSC) (DSC2010, TA instruments) under a heating rate of 10 °C min⁻¹ and a nitrogen flow of 50 mL min⁻¹. The surface morphology of the polymer films was studied using the tapping mode atomic force microscopy (AFM) from a Veeco Nanoscope III controller.

Fabrication and characterization of polymer solar cells

To fabricate the inverted solar cells, ITO-coated glass substrates (15 Ω per \square) were cleaned in sequential ultrasonic baths of detergent water, de-ionized water, acetone, and isopropyl alcohol. Substrates were then treated with the oxygen plasma for 5 min. A thin layer of PCBM-S was prepared by spin-coating the PCBM-S solution (5 mg ml⁻¹ of PCBM-S in chloroform with different amounts of DMC) and then annealed at 200 °C for 30 min in the glove box. Afterward, PCBM (American Dye Source, Inc., 99.0% purity) and P3HT (Rieke Metals, Inc., 4002-E grade) (0.7 : 1, weight ratio) in a chlorobenzene solution (60 mg ml⁻¹) were spin-coated on the PCBM-S layer in a glove box and annealed at 160 °C for 10 min to get an active layer with a thickness of *ca.* 200 nm. After annealing, a PEDOT:PSS solution (H. C. Starck, Clevis 4083) was spin-coated onto the

active layer to get a layer with 50 nm thickness.²⁴ These samples were annealed for 10 min at 120 °C on a hot plate. A metal electrode (Ag) was then vacuum-deposited at a base pressure of 2×10^{-6} Torr at a rate of 2 \AA s^{-1} . The J - V characteristics of the solar cells were tested under ambient conditions using a Keithley 2400 SMU and an Oriel xenon lamp (450 W) with an AM1.5 filter. The device illumination area of 0.0314 cm^2 was defined by using a physical mask to minimize photocurrent generation from the edge of the electrodes. The light intensity was calibrated to 100 mW cm^{-2} using a calibrated silicon solar cell with a KG5 filter, which is traced to the National Renewable Energy Laboratory. The performance of the devices was averaged over at least 5 devices for each processing condition.

Fabrication and characterization of OTFTs

Heavily n-doped silicon substrates with a 300 nm thick thermally grown SiO_2 dielectric (from Montco Silicon Technologies, Inc.) were used to fabricate top contact OTFTs. The substrates were treated with HMDS by vapor phase deposition in a vacuum oven (200 mTorr, 100 °C, 2 hours) before spin-coating of PCBM-S. The undoped and doped PCBM-S films were spin-coated in the glove box. The 1 wt% of PCBM-S in chloroform was used to obtain a film thickness of 50 nm. Interdigitated source and drain electrodes ($W = 9000 \text{ \mu m}$, $L = 90 \text{ \mu m}$, $W/L = 100$) were defined by evaporating a 100 nm Au at 10^{-6} Torr. An Agilent 4155B semiconductor parameter S6 analyzer was used to characterize OTFT properties. The electron mobility was calculated in the saturation regime from the linear fit of $(I_{\text{ds}})^{1/2}$ vs. V_{gs} . The V_{t} was obtained as the x intercept of the linear section of the plot of $(I_{\text{ds}})^{1/2}$ vs. V_{gs} .

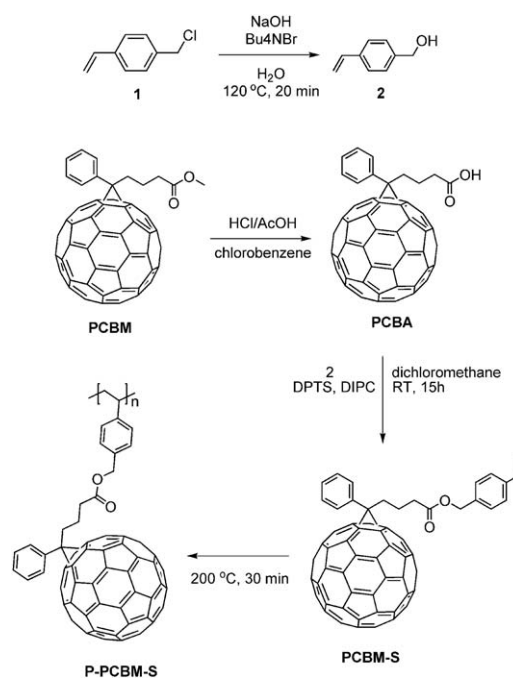
3. Results and discussion

Synthesis and characterization

We have designed PCBM-S to match several requirements as follows. First, the monomer (PCBM-S) should be easily polymerizable in the solid state. Second, the size of the reactive units should be as small as possible to maintain reasonable electron mobility of the polymer. Finally, the polymer film should be insoluble in common organic solvents to allow multilayer solution-processing and the resulting polymer film also need to have good morphological stability during device processing. The PCBM-S was synthesized by the esterification of [6,6]-phenyl- C_{61} -butyric acid (PCBA) with 4-vinyl benzyl alcohol (**2**), as shown in Scheme 1. The PCBM-S was characterized by NMR spectroscopy and elemental analysis.

Thermal properties

The thermal properties of PCBM-S were studied by DSC. As shown in Fig. 1, PCBM-S exhibited a glass-transition temperature (T_g) of 114 °C. After annealing above the T_g , the PCBM-S showed exothermic peaks at 170 °C and 230 °C, which are believed to be the thermal polymerization of styrene linkage.³⁸ In the second scan, these peaks are no longer detectable. This implies that long-range molecular motion of the polymerized PCBM-S (P-PCBM-S) is significantly limited after thermal



Scheme 1 Synthetic route of fullerene polymer.

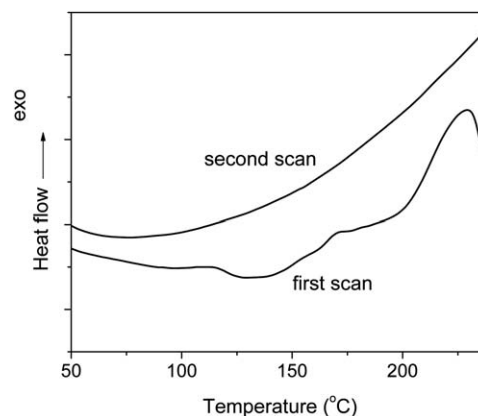


Fig. 1 DSC thermograms of the PCBM-S with a heating rate of $10 \text{ }^\circ\text{C min}^{-1}$.

polymerization and therefore, we expect that the polymer film should have good morphological stability.

Absorption properties

Fig. 2 shows the UV-Vis-NIR absorption spectra of the thin films of undoped and 6 wt% DMC doped PCBM-S on the glass substrate measured before and after washing with chlorobenzene. All films were prepared by spin-coating, then polymerized by thermal annealing at 200 °C for 30 min under inert conditions. The small decrease in the absorption intensities observed for both undoped and 6 wt% DMC doped P-PCBM-S films after rinsing with chlorobenzene demonstrates effective solvent resistance of the films.

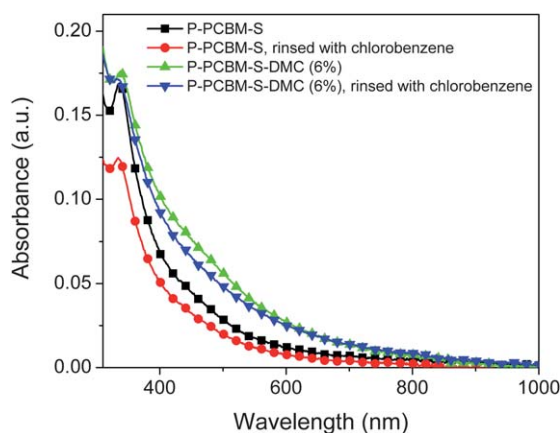


Fig. 2 Absorption spectra of the undoped and DMC doped P-PCBM-S polymer films on glass substrate before and after washing with chlorobenzene.

Photovoltaic properties

Fig. 3 shows the J - V characteristics of inverted polymer solar cells with and without modification of ETM. Devices of architecture ITO/ETM/P3HT:PCBM/PEDOT:PSS/Ag were tested under simulated AM 1.5G illumination at 100 mW cm^{-2} . The results show clear evolution of J - V curves as a function of the doping concentration of DMC in P-PCBM-S films.

A summary of the photovoltaic parameters for the devices is given in Table 1. Note that the PCE increases significantly from 1.24% to 2.53% with an increase in the dopant (DMC) concentration from 0 to 10 wt%. The best performance was obtained from devices with 10 wt% doped PCBM-S. These improvements are attributed from the enhanced electrical conductivity and improved electron extraction efficiency of P-PCBM-S as a result of the increased doping level. As shown in Table 1, the enhanced conductivity of the P-PCBM-S causes an overall decrease in series resistance (R_s) from $1110 \Omega \text{ cm}^2$ for undoped P-PCBM-S to $50 \Omega \text{ cm}^2$ for 10 wt% doped P-PCBM-S, as well as an increase in fill factor (FF) from 0.27 to 0.44. There is also a pronounced enhancement in J_{sc} , V_{oc} , FF, and thus PCE for 3 wt% and 5 wt% doped P-PCBM-S relative to the undoped device. Since there is

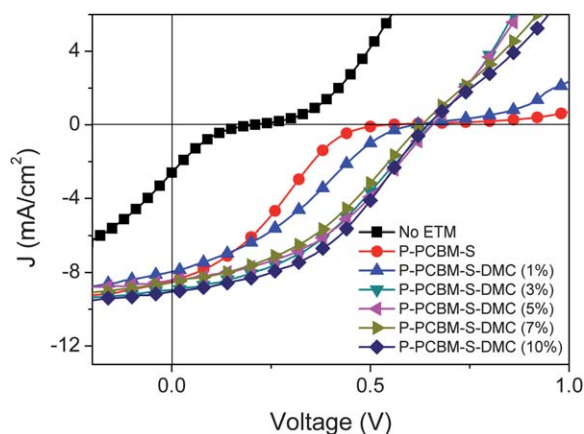


Fig. 3 J - V curves of inverted polymer solar cells as a function of the doping concentration of DMC in P-PCBM-S films.

Table 1 Summary of device performance with various ETMs

ETM	PCE (%)	V_{oc} /V	J_{sc} /mA cm ⁻²	FF	R_s /Ω cm ⁻²
No ETM	0.08	0.21	2.60	0.21	315
P-PCBM-S	1.24	0.54	8.47	0.27	1110
P-PCBM-S-DMC (1%)	1.46	0.61	7.95	0.31	350
P-PCBM-S-DMC (3%)	2.33	0.65	8.96	0.40	40
P-PCBM-S-DMC (5%)	2.32	0.66	8.42	0.42	40
P-PCBM-S-DMC (7%)	2.16	0.63	8.53	0.40	50
P-PCBM-S-DMC (10%)	2.53	0.64	9.06	0.44	50

no significant increase in PCE of the 10 wt% doped device compared to the 3–5 wt% doped device, we suggest that 3–5 wt% is an effective doping concentration for present experiments. The slight variation in PCE of devices doped with higher concentration of DMC (7 and 10 wt%) can be attributed to the unoptimized morphology of the electron transport layers.

Morphology

The ability of controlling the thickness and morphology of the electron-transporting layer (ETL) is very important for optimizing device performance since the series resistance across the device is strongly dependent on the thickness of the ETL. In addition, a smooth and pinhole free ETL film prevents the leakage current at the interface and plays a crucial role in the lifetime and efficiencies of PSCs. To investigate how the morphology of the P-PCBM-S film affects the device performance, we studied the surface morphology of n-doped P-PCBM-S films prepared under different spin coating conditions and evaluated the corresponding device performance.

Devices based on 3 wt% DMC doped P-PCBM-S films spin-coated by 7000 rpm show almost the same device performance (PCE: 2.30%, V_{oc} : 0.65 V, J_{sc} : 8.90 mA cm⁻²; FF: 0.41) with the devices spin-coated by 4000 rpm (PCE: 2.33%, V_{oc} : 0.65 V, J_{sc} : 8.96 mA cm⁻², FF: 0.40). However, decreasing the spin speed to 2000 rpm results in shorting of devices. This shorting results from the poor morphology that originates from dewetting between the P-PCBM-S layer and ITO. The significant morphological differences of n-doped P-PCBM-S films as a function of the spin speed were investigated by AFM (Fig. 4).

The DMC doped P-PCBM-S films spin-coated at 2000 rpm have a very rough surface (9.7 rms) due to dewetting, whereas the films spin-coated by the speed of 4000 and 7000 rpm give relatively smooth surfaces (4.0 rms and 2.7 rms, respectively). The surface morphology of the P3HT:PCBM active layer deposited on the interfacial layers prepared under different spin coating conditions shows no observable change in the surface morphology. It is probably due to the relatively thick BHJ film (~200 nm) used in our study, making its morphology less sensitive to the underlying interfacial layer. This further suggests that the major reason for the poor performance of the device with the rough P-PCBM-S film prepared at lower spin speed is due to the potential formation of shorting paths between the ITO substrate and BHJ film, which resulted in electrical leakage at the interface.

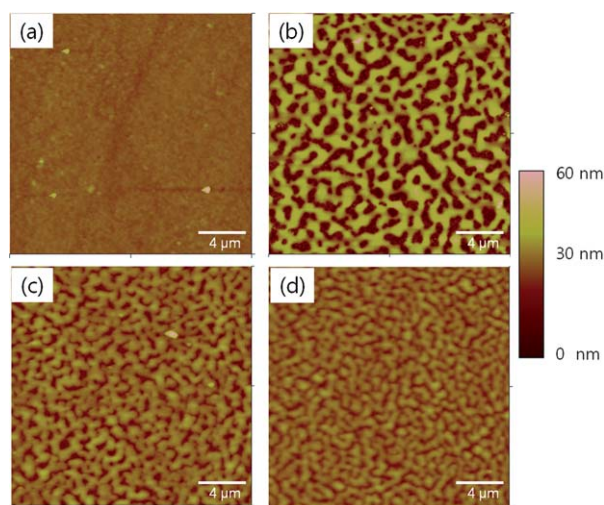


Fig. 4 AFM images of P-PCBM-S (a), 3% DMC doped P-PCBM-S cast by different spin speeds: 2000 rpm (b), 4000 rpm (c), and 7000 rpm (d).

There are two plausible mechanisms that could explain the dewetting of the film spin-coated at the speed of 2000 rpm. One is that the surface energy of the P-PCBM-S film could be significantly changed by DMC compared to the undoped P-PCBM-S film. Compared to doped P-PCBM-S films, undoped P-PCBM-S films on ITO show low surface roughness (1–1.5 rms) regardless of the spin speeds. Another reason for the morphological difference from different spin speed is that the faster solvent evaporation rate at higher spin speed may alter the drying kinetics of the film, which resulted in smoother film by suppressing the dewetting property.³⁹

Organic field-effect transistors

The electrical conductivity of the charge transport materials used in polymer solar cells is an important factor that governs the performance of the devices. Thus, we further investigated the electron-transporting properties of n-doped P-PCBM-S *via* the fabrication of n-type OTFTs. The 1, 3, 5, 7 and 10 wt% of DMC doped PCBM-S solutions were prepared by the same method used for fabricating solar cells. The n-doped PCBM-S solutions were spin-coated onto a heavily doped n++ Si wafer with a 200 nm thick SiO₂ layer with a top contact geometry and Au was used as the source and drain electrodes (*see the Experimental section for detailed fabrication protocols*).

With increasing the doping concentration from 0 to 3% in P-PCBM-S films, the OTFT devices showed well known doping effects such as the negative shift of threshold voltages and the decrease of on–off ratio as shown in Fig. 5(a) and Table 2.⁴⁰ The device with undoped P-PCBM-S shows field-dependent transfer characteristics, whereas the devices with highly doped (5–10 wt %) P-PCBM-S exhibit field-independent properties with small $I_{\text{on}}/I_{\text{off}}$ ratio of <10, which is a characteristic of conducting materials. In addition, Fig. 5(b) clearly shows that the output current of devices at zero gate bias condition increased upon increasing the amount of dopant, indicating that the doping concentration directly affects the amount of charge carriers and

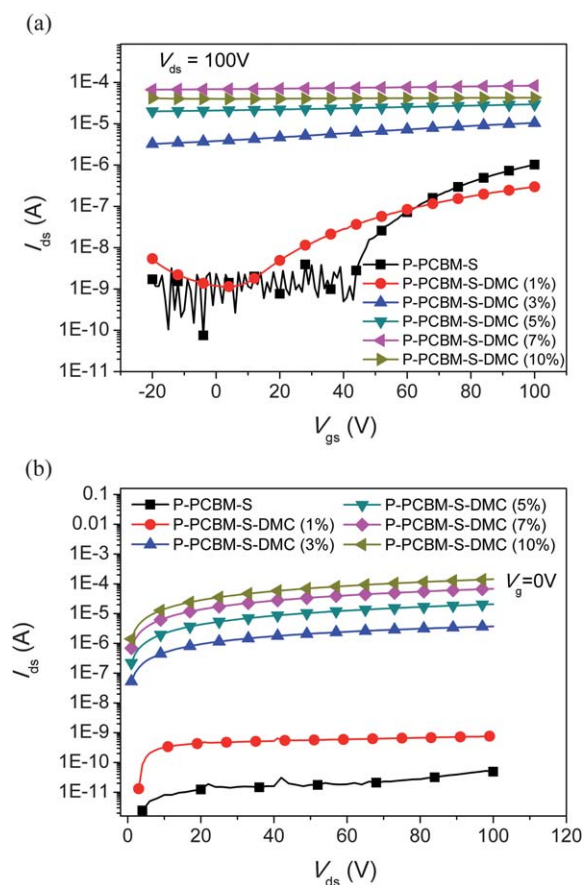


Fig. 5 (a) Transfer characteristics of OTFTs with undoped and DMC doped P-PCBM-S as active layers at varying doping concentrations. (b) Output curves at zero gate voltages for the same devices.

Table 2 OTFT electrical properties for undoped and DMC doped P-PCBM-S transistors at different doping concentrations measured in the N₂-filled glove box

ETM	$\mu/\text{cm}^2 \text{V}^{-1} \text{s}^{-1}$	$I_{\text{on}}/I_{\text{off}}$	V_t/V	$\sigma/\text{S m}^{-1}$
P-PCBM-S	1.45×10^{-4}	10^3	42.0	1.65×10^{-7}
P-PCBM-S–DMC (1%)	1.35×10^{-5}	10^2	6.8	1.53×10^{-6}
P-PCBM-S–DMC (3%)	2.76×10^{-5}	10	–20.2	1.43×10^{-2}
P-PCBM-S–DMC (5%)	—	<10	—	8.54×10^{-2}
P-PCBM-S–DMC (7%)	—	<10	—	2.84×10^{-1}
P-PCBM-S–DMC (10%)	—	<10	—	5.96×10^{-1}

is responsible for the increased electrical conductivity of the doped P-PCBM-S films.

The conductivity of the films was derived from gated two-terminal measurements and the conductivity can be calculated from the equation of $\sigma(V_g) = (L/A)(I_d/V_d)$, where L and A are the channel length and the cross-sectional area of the device, respectively. The conductivities calculated from the slope of V_d – I_d curves at zero gate voltage are summarized in Table 2. There is a pronounced enhancement in the conductivity of $1.65 \times 10^{-7} \text{ S cm}^{-1}$ for undoped P-PCBM-S to $5.96 \times 10^{-1} \text{ S cm}^{-1}$ for 10 wt% doped P-PCBM-S. These values are comparable with previously reported results.⁴⁰ Moreover, the overall trend of the increased

output current with doping concentration is well matched with the decrease of series resistance in the solar cells (Table 1).

For example, there are significant improvements in both the output current of OTFT devices and series resistance of solar cell devices from 1% doped P-PCBM-S to 3% doped P-PCBM-S. However, they are saturated after 3% of the doping concentration. In particular, the annealed device with 10% of DMC in P-PCBM-S shown in Fig. 5(b) had more than 6 orders of magnitude higher drain current than that of the device with undoped P-PCBM-S. The systematic transition of device characteristics including threshold voltage (V_t), conductivity, and on-off current ratio (I_{on}/I_{off}) as a function of the doping concentration is obvious and it further elucidates the relationship between the electrical properties of the n-doped P-PCBM-S layers and the device performance of solar cells.

4. Conclusion

A new thermally polymerizable fullerene derivative has been synthesized to explore its use as an interfacial electron-transporting material for inverted polymer solar cells. The key advantage of this fullerene polymer (P-PCBM-S) is that it enables multi-layer solution processing and facilitates cascade electron transport for efficient electron collection in PSCs. It was demonstrated that chemical n-doping of P-PCBM-S almost double the power conversion efficiency of inverted devices. The improved device performance is attributed to the decreased series resistance and efficient electron extraction from the active layer through the n-doped P-PCBM-S interfacial layer.

Acknowledgements

The authors thank the support from the National Science Foundation (DMR-0120967), the Department of Energy (DE-FC3608GO18024/A000), the AFOSR (FA9550-09-1-0426), the Office of Naval Research (N00014-11-1-0300), and the World Class University (WCU) program through the National Research Foundation of Korea under the Ministry of Education, Science and Technology (R31-21410035). A.K.-Y.J. thanks the Boeing Foundation for support.

References

- 1 C. Brabec, N. Sariciftci and J. Hummelen, *Adv. Funct. Mater.*, 2001, **11**, 15.
- 2 G. Yu, J. Gao, J. Hummelen, F. Wudl and A. Heeger, *Science*, 1995, **270**, 1789.
- 3 J. Halls, C. Walsh, N. Greenham, E. Marseglia, R. Friend, S. Moratti and A. Holmes, *Nature*, 1995, **376**, 498.
- 4 H. Chen, J. Hou, S. Zhang, Y. Liang, G. Yang, Y. Yang, L. Yu, Y. Wu and G. Li, *Nat. Photonics*, 2009, **3**, 649.
- 5 Y. Liang, Z. Xu, J. Xia, S. Tsai, Y. Wu, G. Li, C. Ray and L. Yu, *Adv. Mater.*, 2010, **22**, E135.
- 6 Y. Li and Y. Zou, *Adv. Mater.*, 2008, **20**, 2952.
- 7 J. Hou, H. Chen, S. Zhang, G. Li and Y. Yang, *J. Am. Chem. Soc.*, 2008, **130**, 16144.
- 8 Y. Liang, Y. Wu, D. Feng, S. Tsai, H. Son, G. Li and L. Yu, *J. Am. Chem. Soc.*, 2009, **131**, 56.
- 9 R. Coffin, J. Peet, J. Rogers and G. Bazan, *Nat. Chem.*, 2009, **1**, 657.
- 10 P. Troshin, H. Hoppe, J. Renz, M. Egginger, J. Mayorova, A. Goryachev, A. Peregudov, R. Lyubovskaya, G. Gobsch and N. Sariciftci, *Adv. Funct. Mater.*, 2009, **19**, 779.
- 11 C. Yang, J. Kim, S. Cho, J. Lee, A. Heeger and F. Wudl, *J. Am. Chem. Soc.*, 2008, **130**, 6444.
- 12 J. Peet, J. Kim, N. Coates, W. Ma, D. Moses, A. Heeger and G. Bazan, *Nat. Mater.*, 2007, **6**, 497.
- 13 G. Li, Y. Yao, H. Yang, V. Shrotriya, G. Yang and Y. Yang, *Adv. Funct. Mater.*, 2007, **17**, 1636.
- 14 W. Ma, C. Yang, X. Gong, K. Lee and A. Heeger, *Adv. Funct. Mater.*, 2005, **15**, 1617.
- 15 M. Jørgensen, K. Norrman and F. Krebs, *Sol. Energy Mater. Sol. Cells*, 2008, **92**, 686.
- 16 S. K. Hau, H. L. Yip, H. Ma and A. K. Y. Jen, *Appl. Phys. Lett.*, 2008, **93**, 233304.
- 17 S. K. Hau, H. L. Yip, K. Leong and A. K. Y. Jen, *Org. Electron.*, 2009, **10**, 719.
- 18 C. Waldauf, M. Morana, P. Denk, P. Schilinsky, K. Coakley, S. A. Choulis and C. J. Brabec, *Appl. Phys. Lett.*, 2006, **89**, 3.
- 19 M. S. White, D. C. Olson, S. E. Shaheen, N. Kopidakis and D. S. Ginley, *Appl. Phys. Lett.*, 2006, **89**, 143517.
- 20 S. K. Hau, H. L. Yip, N. S. Baek, J. Y. Zou, K. O'Malley and A. K. Y. Jen, *Appl. Phys. Lett.*, 2008, **92**, 253301.
- 21 T. Kuwabara, Y. Kawahara, T. Yamaguchi and K. Takahashi, *ACS Appl. Mater. Interfaces*, 2009, **1**, 2107.
- 22 Y. Z. Jin, J. P. Wang, B. Q. Sun, J. C. Blakesley and N. C. Greenham, *Nano Lett.*, 2008, **8**, 1649.
- 23 D. Ko, J. Tumbleston, M. Ok, H. Chun, R. Lopez and E. Samulski, *J. Appl. Phys.*, 2010, **108**, 083101.
- 24 S. K. Hau, H. L. Yip, O. Acton, N. S. Baek, H. Ma and A. K. Y. Jen, *J. Mater. Chem.*, 2008, **18**, 5113.
- 25 S. K. Hau, Y. J. Cheng, H. L. Yip, Y. Zhang, H. Ma and A. K. Y. Jen, *ACS Appl. Mater. Interfaces*, 2010, **2**, 1892.
- 26 C. H. Hsieh, Y. J. Cheng, P. J. Li, C. H. Chen, M. Dubosc, R. M. Liang and C. S. Hsu, *J. Am. Chem. Soc.*, 2010, **132**, 4887.
- 27 Y. H. Zhou, H. Cheun, W. J. Potscavage, C. Fuentes-Hernandez, S. J. Kim and B. Kippelen, *J. Mater. Chem.*, 2010, **20**, 6189.
- 28 H. H. Liao, L. M. Chen, Z. Xu, G. Li and Y. Yang, *Appl. Phys. Lett.*, 2008, **92**, 173303.
- 29 A. G. Werner, F. Li, K. Harada, M. Pfeiffer, T. Fritz and K. Leo, *Appl. Phys. Lett.*, 2003, **82**, 4495.
- 30 F. Huang, Y. J. Cheng, Y. Zhang, M. S. Liu and A. K. Y. Jen, *J. Mater. Chem.*, 2008, **18**, 4495.
- 31 A. W. Hains and T. J. Marks, *Appl. Phys. Lett.*, 2008, **92**, 023504.
- 32 A. W. Hains, J. Liu, A. B. F. Martinson, M. D. Irwin and T. J. Marks, *Adv. Funct. Mater.*, 2010, **20**, 595.
- 33 Y. Sun, X. Gong, B. B. Y. Hsu, H. L. Yip, A. K. Y. Jen and A. J. Heeger, *Appl. Phys. Lett.*, 2010, **97**, 193310.
- 34 C. Chan, W. Zhao, A. Kahn and I. Hill, *Appl. Phys. Lett.*, 2009, **94**, 203306.
- 35 D. V. Konarev, S. S. Khasanov, G. Saito, I. I. Vorontsov, A. Otsuka, R. N. Lyubovskaya and Y. M. Antipin, *Inorg. Chem.*, 2003, **42**, 3706.
- 36 R. He, P. Toy and Y. Lam, *Adv. Synth. Catal.*, 2008, **350**, 54.
- 37 J. Hummelen, B. Knight, F. LePeq, F. Wudl, J. Yao and C. Wilkins, *J. Org. Chem.*, 1995, **60**, 532.
- 38 G. Klarner, J. Lee, V. Lee, E. Chan, J. Chen, A. Nelson, D. Markiewicz, R. Siemens, J. Scott and R. Miller, *Chem. Mater.*, 1999, **11**, 1800.
- 39 S. Y. Heriot and R. A. L. Jones, *Nat. Mater.*, 2005, **4**, 782.
- 40 P. Wei, J. Oh, G. Dong and Z. Bao, *J. Am. Chem. Soc.*, 2010, **132**, 8852.